Reflections in traveling wave tubes : Simulation using the 1-D time domain Hamiltonian model DIMOHA with experimental validation

Khalil Aliane, Fréderic André, Yves Elskens

Reflections in Traveling Wave Tubes : Simulation Using the 1-D Time Domain Hamiltonian Model DIMOHA with Experimental Validation

Khalil Aliane, Frédéric André, Yves Elskens

***Abstract*— DIMOHA is a many-particle time domain model offering a good balance between exhaustive physics and time efficiency. We apply this model to study the effects of defects and reflections in the slow wave structure of a traveling wave tube. To assess DIMOHA's validity, we set up a traveling wave tube with varying reflection coefficient at the tube's end. A ripple effect in saturated output power with respect to frequency is measured and simulated self-consistently with a rough agreement.**

I. Introduction

While traveling wave tubes (TWTs) are always supported by periodic wave-guides, be it coupled cavities or helical wave-guides amongst others, they are still home for several discontinuities, from the non-uniform pitch profile (taper), to the local attenuators, and, most prominently, imperfect adaptations at both ends of the slow wave structure. Each one of these discontinuities can cause propagating radio-frequency (RF) waves to be partially reflected, potentially affecting the TWT's proper functioning.

Reflected waves can indeed deteriorate the stability of the TWT [1], cause overheating while being absorbed in the attenuators, and diminish the TWT gain. For the latter point, the partially reflected RF power will trivially be missing from the gain output. This however is complicated if the reflected wave is in turn partially reflected on the attenuator, in which case it will interfere with the initial direct wave. The section between the TWT end and the attenuator's end thus acts as a resonant cavity, similarly to a Fabry-Pérot interferometer. If the electrical length of a cavity, that is the ratio $2L/\lambda$ where λ is the wavelength and $2L$ the roundtrip length of the cavity, is an integer, the initial and the twice partially reflected waves are perfectly in phase, and the interference is constructive. Oppositely, for a half-integer electric length, the two interfering waves are in phase opposition, and thus cancel each other, the interference is destructive. This mechanism leads to a ripple in the output RF power along the frequency bandwidth (see figure 1), characterised with a period

$$\Delta f = \frac{v_g}{2L}. \tag{1}$$

where the group velocity v_g is assumed to remain approximately constant over the bandwidth of interest.

Studies of such reflections have been conducted using frequency domain models [1]–[5], some of which include experimental scrutiny [5]–[7]. However, frequency domain methods, while offering very fast simulations, are not best suited for such a phenomenon. Indeed, intricate methods and algorithms need to be carried out to ensure consistency for multi-frequency operations; most problematically perhaps for complex non-linear interactions and transient phenomena.

On the other hand, while time domain models, such as Particle-In-Cell (PIC) codes, offer a self-consistent and straightforward way to incorporate reflections, their larger required time and CPU costs make them impractical. In recent years however, a new class of time-domain models emerged, showing a promising balance between exhaustive physics modeling and reasonable computing time cost.

One such model, DIMOHA, uses a particular electromagnetic field decomposition in order to considerably reduce the number of degrees of freedom, and proved to be particularly flexible and versatile [8]–[10]. In this article, we propose to implement and assess this model for and with the study of reflections in a TWT, in particular the power ripple caused by such reflections.

To strengthen our study, we compare DIMOHA's simulations with measurements taken from a well adapted TWT equipped with adjustable reflection levels, specifically set up for this purpose, rather than relying on defective or flawed TWTs.

Note that all data points shown in the plots represent actual data, either from DIMOHA's simulations or measurements. The lines connecting these points are interpolations intended to guide the eye and enhance the readability of the figures.

II. Measurements

In order to validate our reflection model, and to further examine the effects of reflections in a traveling wave tube, we carried out measurements on a TWT at saturation with varying standing wave ratio (SWR). The setup consists of a Ku-band TWT attached to a basic rectangular wave-guide, perforated at the top (fig. 2). The slot at the top of the rectangular wave-guide allows us to insert a metallic reflective obstacle. The depth at which the obstacle is inserted can be adjusted using a scroll wheel, thusly adjusting the level of reflections in the

K. Aliane was with the Centre National d'Études Spatiales, Toulouse, France (khalil.aliane@univ-amu.fr).

K. Aliane and Y. Elskens (yves.elskens@univ-amu.fr) are with Aix-Marseille Université, CNRS, UMR 7345 PIIM, Marseille, France.

K. Aliane was and F. André (frederic.andre@thalesgroup.com) is with Thales AVS, Vélizy-Villacoublay, France.

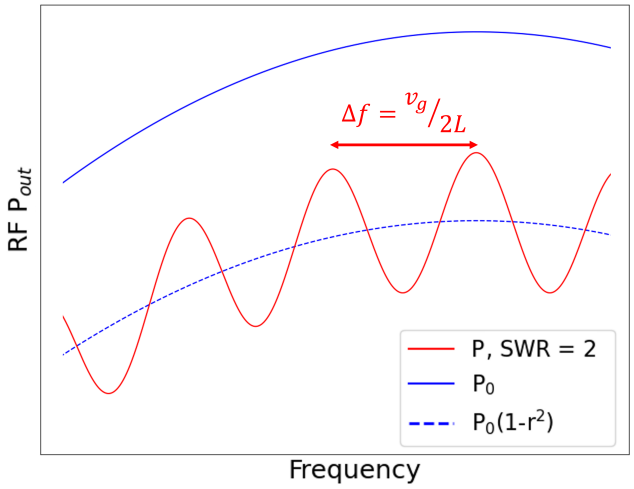

Fig. 1. Illustration of the ripple effect on the RF output power in respect to frequency : in plain blue the RF output power with no reflection P_0, and in dotted blue the RF power with a given reflection coefficient r at the exit. If the reflected wave is in turn reflected on the attenuator, the RF power (in red) oscillates around $(1 - r^2)P_0$.

TWT. The reference measurements P_0 with no reflections are taken with the obstacle probe completely outside the slot. The distance between the TWT exit and the obstacle is neglected for all purposes, since the RF waves propagate at the speed of light in this short section.

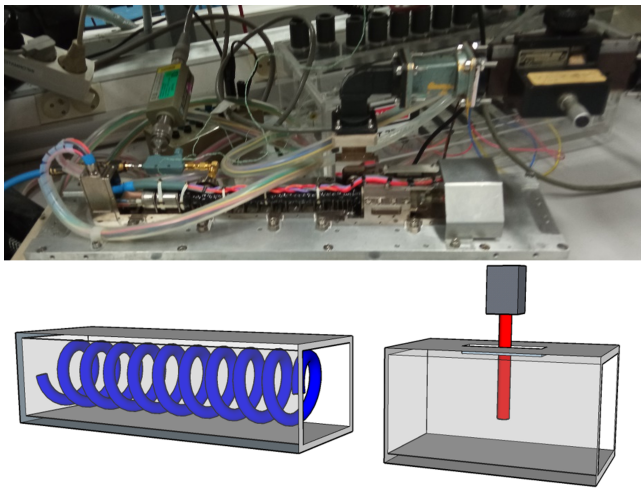

Fig. 2. Experimental setup : A TWT is attached to a perforated rectangular wave-guide with an insertable metallic probe.

First, to characterise the adjustable probe, we map each depth to the standing wave ratio. This is carried out by measuring the standing wave ratios with the TWT off using a vector network analyzer. Figure 3 shows the measured SWR as a function of the RF input frequency for several depths of the probe. The test setup without the probe is characterized by a maximum SWR$= 1.03$, whereas by inserting the metallic probe to the maximum, we achieve a SWR of ~ 2, i.e. about a ninth of the RF power is reflected. Reflection levels fluctuate across the frequency bandwidth, though these variations are limited below 5%. Furthermore, the frequency profile in fig. 3 does not depend on the probe's depth.

Note that the legends of figures 3 and 4 indicate the height of the probe above the bottom of the rectangular wave-guide, rather than the insertion depth. Thus, a height of 0.0 mm corresponds to the probe being inserted to its maximum depth.

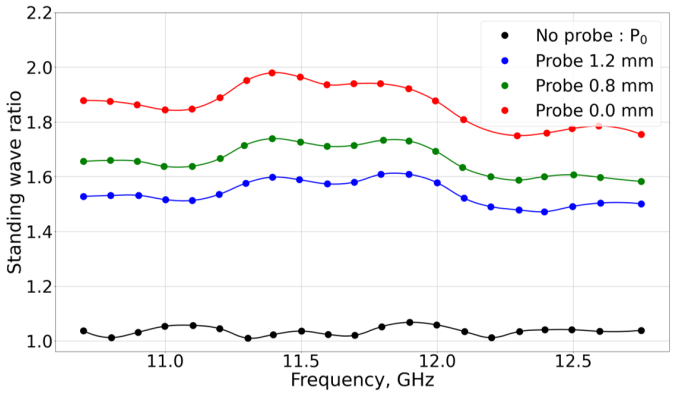

Fig. 3. Cold standing wave ratio frequency profile, measured for several configurations of the probe.

Once the reflective probe is characterised, the saturated RF output power is measured at the exit of the setup across all the bandwidth $10.75 - 12.75$ GHz. Figure 4 shows the saturated RF output power as a function of frequency for several probe depths, in other words for various reflection levels. The ripple is apparent. Furthermore, the deeper the probe, the larger the ripple's amplitude, whereas the ripple's period is the same. This comes as no surprise since the latter depends only on the electric length of the resonant cavity created between the attenuator's end and the probe.

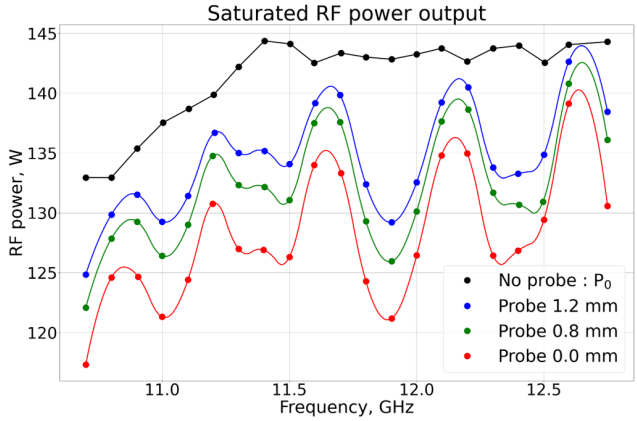

Fig. 4. RF output power as a function of frequency, measured for several configurations of the probe. The red points correspond to the maximum insertion of the probe, i.e., the maximum reflections.

We note that the measured ripple's period is greater than the theoretical estimate of 0.4 GHz (1). Additionally, it varies by up to 15% across the bandwidth, despite the group velocity remaining nearly constant. This discrepancy may be attributed to external reflections or limitations in measurement accuracy. Specifically, the looseness of the metallic probe makes it challenging to maintain a fixed cavity length. Given the wavelengths involved, even slight deviations of a few millimeters

can cause noticeable differences.

III. Modeling

A more thorough description of DIMOHA is given in [9]. DIMOHA is a one-dimensional time domain multi-particle hamiltonian model. The time cost problem often encountered with such models is solved through a peculiar field decomposition known as Kuznetsov discrete model which allows to describe periodic structures using a number of degrees of freedom equal to the number of spatial periods of said structure.

In this discrete model, the electromagnetic fields are decomposed as

$$\mathbf{E}(\mathbf{r},t) = \frac{1}{2\pi}\int_{-\pi}^{\pi} V_\beta(t)\,\mathbf{E}_\beta(\mathbf{r})\,\mathrm{d}(\beta d), \tag{2a}$$

$$\mathbf{H}(\mathbf{r},t) = \frac{\mathrm{i}}{2\pi}\int_{-\pi}^{\pi} I_\beta(t)\,\mathbf{H}_\beta(\mathbf{r})\,\mathrm{d}(\beta d), \tag{2b}$$

where V_β and I_β are time-dependent amplitudes, factor i results from a technical convention, and d is the period (e.g. the pitch for a helix). The eigenfields $\mathbf{E}_\beta$, $\mathbf{H}_\beta$ are solutions to the Helmholtz equations, they depend only on the slow wave structure (SWS) geometry and contain dispersion and coupling properties. This representation, known as Gel'fand transform, is mixed, meaning it allows for spatial and spectral dependence. Here lies the other asset of DIMOHA : while this discrete model is built for perfectly periodic SWS, it is flexible enough to allow for spatial discontinuities, as long as they are not too steep. This makes it ideal for simulating tapered TWTs, or, of more interest for this work, local reflections.

The cold propagation scheme for DIMOHA, derived from the source-free Maxwell equations, reads

$$\partial_t V_\beta(t) = -\omega_\beta I_\beta(t), \tag{3a}$$

$$\partial_t I_\beta(t) = \omega_\beta V_\beta(t), \tag{3b}$$

where ω_β is the time pulsation for the spectral component β, the dependence between the two defines the dispersion relation of the structure. Using the inverse Gel'fand transform, we obtain the cold propagation equations in space representation

$$\mathrm{d}_t V_n(t) = -\sum_m \Omega_m^n I_m(t), \tag{4a}$$

$$\mathrm{d}_t I_n(t) = \sum_m \Omega_m^n V_m(t), \tag{4b}$$

with (V_n, I_n) the inverse Gel'fand transforms of (V_β, I_β)

$$(V_n, I_n) = \frac{1}{2\pi}\int_{-\pi}^{\pi} (V_\beta, I_\beta)\,\mathrm{e}^{-\mathrm{i}\beta n d}\,\mathrm{d}(\beta d). \tag{5}$$

Equations (4) describe a chain of coupled harmonic oscillators with the coupling coefficients Ω_m^n deriving from the dispersion relation ω_β :

$$\Omega_m^n = \frac{1}{2\pi}\int_{-\pi}^{\pi} \omega_\beta\,\mathrm{e}^{-\mathrm{i}\beta(n-m)d}\,\mathrm{d}(\beta d). \tag{6}$$

The local nature of these coefficients allows us to truncate the coupling range N_{ph} down to a few cells.

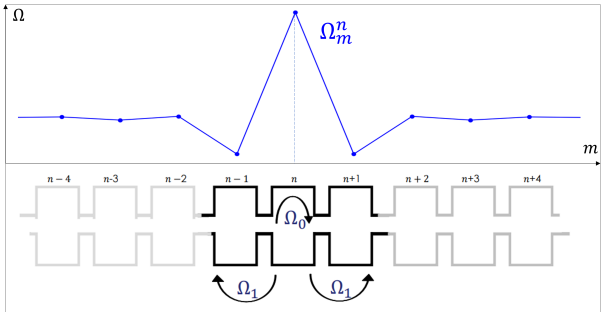

Fig. 5. Illustration of DIMOHA's propagation scheme.

In this frame of work, where the propagation properties are governed by the coupling coefficients Ω_m^n, one can include tapers simply by altering those coefficient from cell to cell, so as to reproduce different dispersion relations $\omega_\beta^{(n)}$ for each cell. This has been done in [10], [11], where DIMOHA was successfully tested with tapered industrial TWTs. Note that if the change in the coefficients is too abrupt, it may induce reflections.

Using the same underlying principle, if we aim to deliberately introduce reflections within a slow-wave structure (SWS) at a discontinuous interface located at a given point z_0, we can intentionally modify the coupling coefficients around this point to achieve the desired reflection rate [12].

If we distribute the effect of this defect over N_{ph} cells to the left and right of z_0, it becomes necessary to adjust $2N_{\mathrm{ph}}(2N_{\mathrm{ph}}+1)$ coupling coefficients. This adjustment would require us to define $\frac{N_{\mathrm{ph}}(2N_{\mathrm{ph}}+1)}{2}$ data points for the reflection and transmission coefficients $r_{\mathrm{d}}(\omega_\beta)$ and $t_{\mathrm{d}}(\omega_\beta)$. Moreover, if the goal is to capture slight variations in r_{d} over a narrow frequency range, increasing the coupling range N_{ph} might be necessary.

However, if the frequency dependence of r_{d} is not critical, one can still achieve satisfactory results by adjusting only the $2N_{\mathrm{ph}}+1$ coupling coefficients of the cell closest to the defect position z_0.

Additionally, since the typical dispersion relation $\omega(\beta)$ for a TWT is almost linear away from the Brillouin zone boundaries, the coupling coefficients Ω_m^n decrease as $1/(n-m)^2$ [9] (as shown in Figure 5). This means that propagation properties are predominantly influenced by the self-coupling coefficient Ω_0^0. Consequently, in this study, we only altered the self-coupling coefficient near the exit $\Omega_{n_{\mathrm{out}}}^{n_{\mathrm{out}}}$ by multiplying it with a factor that we adjusted to fit the measured standing wave ratio (SWR). It should be noted that by doing so, we forgo control over the frequency profile of the reflections $r_{\mathrm{d}}(\omega)$.

Figure 7 compares the measured and simulated SWRs for the case with the maximum depth (SWR $\sim$ 2). Using this simplified method, DIMOHA reproduces the measurements with an accuracy of approximately 5%.

Note that in order to insure the back and forth propagation between the output and the attenuator in DIMOHA, we need to introduce some reflection at the attenuator's end by slightly altering the coupling coefficient of the corresponding cell in addition to the output cell. One way to visualise this back-and-forth is by looking at the RF power along the tube, with

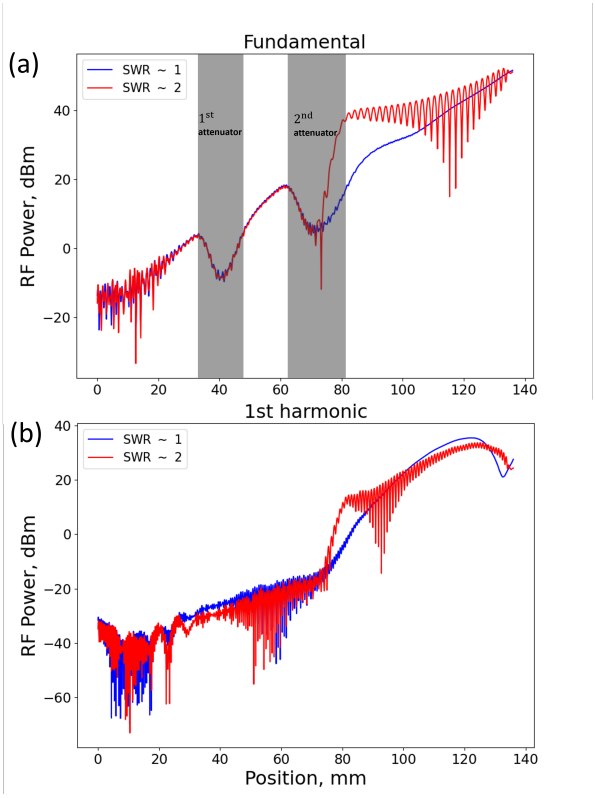

Fig. 6. RF power for a given drive frequency ($f = 11.2$ GHz) along the slow wave structure for the fundamental (top) and the first harmonic (bottom) : DIMOHA's simulations with (red) and without (blue) the defect (here the SWR of the defective exit cell ~ 2).

and without the defect at the exit (see fig. 6.a).

Finally, the previous discussion only concerns the deliberate inclusion of reflections and does not address boundary conditions. In DIMOHA, these are managed by setting a perfectly matched layer (PML), which consists of absorbing layers at both ends of the delay line. While the PML is adjusted to prevent the reflection of the cold fields at the exit, the presence of the beam can induce some spurious reflections [4]. However, these can be eliminated in DIMOHA by extending the simulated delay line beyond its physical length and gradually decreasing the beam-wave interaction before reaching the PML.

IV. Simulations and Measurements Comparison

Once we determined the cold parameters, we simulate both the saturated and small signal output power for the standard (SWR$=1.0$) and defective (SWR~ 2) configurations, across the frequency bandwidth. For a given frequency, several (~ 20) simulation runs are required to scout the input power range and thus insure that we reached saturation; repeating this operation for all frequencies necessitated around 200 simulations. Such a study would have been impossible using a standard multi-particle time domain PIC-like code. However, thanks to its order reduction, one DIMOHA simulation takes less than one minute for such a TWT. Note that saturation does not necessarily occur at the same input power for the standard and defective cases; indeed, as the electrons in presence of a reflected wave experience either more or less RF field depending on the nature of the interferences, they get trapped either sooner or later than in the standard scenario.

As shown in Figure 8, DIMOHA successfully reproduces the RF power ripple. While the simulated ripple amplitude matches the measured value, the periods of the measured and simulated ripples differ. The simulated ripple period aligns more closely with the theoretical estimate (1), displaying an approximately constant period of 0.4 GHz across the entire bandwidth.

The measured ripple period is consistently longer than both the simulated and estimated periods. As previously noted, this discrepancy could be due to an incorrect estimation of the electrical length. This misestimation might stem from inaccuracies in determining the physical distance between the probe and the sever's end, or in estimating the group velocity in the delay line. Indeed, the dispersion properties employed in DIMOHA are based on electromagnetic simulations of the TWT rather than on direct measurements.

It also is important to note that since the defective probe is simulated by modifying the output cell coefficient, its position is estimated with an error margin of up to half a cell (i.e., half the helix pitch). The same uncertainty applies to the altered attenuator's end cell. As a result, both the electrical length and the positions of the simulated ripple peaks are highly approximate. Furthermore, the rectangular wave-guide section is not accounted for in DIMOHA. However, as previously noted, this omission is unlikely to have a significant impact, since the RF fields propagate at the speed of light in that section. If anything, a longer wave-guide section would result in a smaller ripple period, not the opposite.

Finally, these discrepancies might also stem from additional sources of reflections, both within and outside the TWT, that were not considered in the theoretical estimate (1) or in DIMOHA's simulations. One such reflection may arise from backward-traveling electrons originating from the collector, which induce a backward signal in the delay line. This signal can be reflected at the sever's exit, contributing to the RF power ripple and altering its period.

Note that the ripple in RF power is mirrored in the electrons velocity distribution function at the end of the TWT, as can be seen in figures 9. The electron velocity distribution function is obtained by normalizing electrons velocity distribution at the exit so that the integral over the velocity range is 1.

Figure 10 compares the simulated output power with and without reflections in the small signal regime. Two key observations can be made. First the ripple's relative amplitude is significantly larger than in the saturated case. This comes as no surprise, since an increase or decrease in the RF power in the line results in a proportional change in output power, unlike in the saturated scenario.

Second, more interestingly, both saturated and small signal results share more or less the same frequency dependence; the ripple period fits well with the simple model 1.

This goes against previous studies [7] where it was shown that for several L-band, C-band and Ka-band TWTs, the ripple's period in large signal regimes $\frac{1}{2}\Delta f$ is half that of the small signals Δf in the output power vs drive frequency

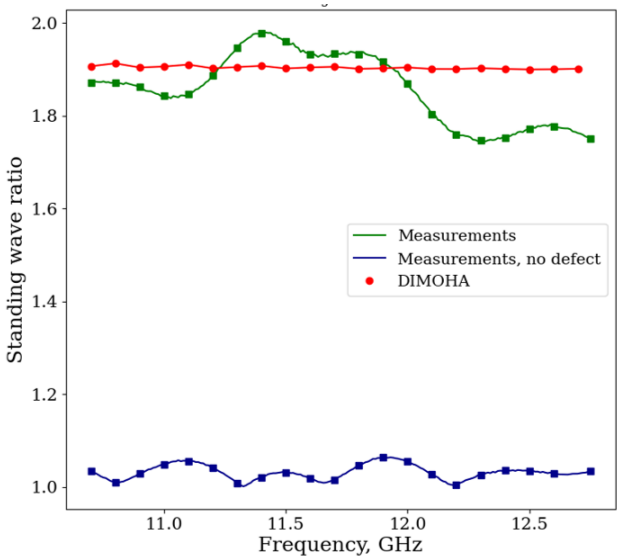

Fig. 7. Cold standing wave ratio : measurements (green) and simulations (red) for the maximum depth of the probe, measurements for the no-reflection test setup (blue).

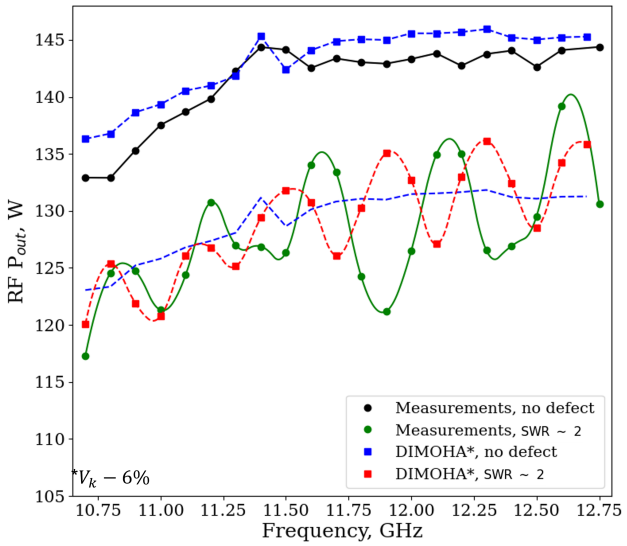

Fig. 8. RF output power as function of frequency : measurements (black) and simulations (blue) for the standard setup, and for the maximum SWR setup (green and red respectively).

curve.

This is due to the strong presence of harmonics in the line, viz. integer multiples of the signal's fundamental frequency, generated as a result of nonlinear interactions with the beam. The factor of $\frac{1}{2}$ highlights the prevalence of the first harmonic, i.e., $f_1 = 2f$.

In our case, due to the low harmonic levels in the Ku-band TWT (see fig.6.b), and to the strong reflections, the measured and simulated ripple is driven by the fundamental drive frequency, even at saturation.

V. Conclusion

While multi-particle time-domain self-consistent simulations are appropriate to model the complex multi-frequency

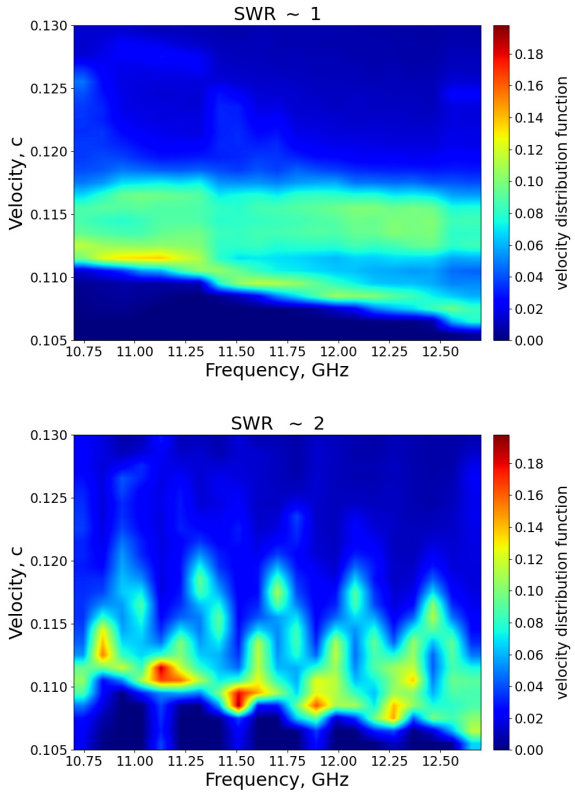

Fig. 9. Simulated steady-state electronic velocity distribution functions at the TWT's exit as function of frequency for the standard (top), and maximum SWR (bottom) setup.

wave-beam interactions in a TWT, including discontinuities and multi-reflections, their benefits can quickly be outweighed by their time cost, considerably larger than frequency-domain simulations. Using an order reduction model, the Kuznetsov discrete decomposition, DIMOHA, a 1-D hamiltonian time domain model, addresses this problem by reducing considerably the number of degrees of freedom, hence reducing the simulation time and memory cost.

In this article, we used DIMOHA to simulate and study the effect of reflections in a TWT. We showed that thanks to its optimal discrete field decomposition, and by virtue of being in time domain, DIMOHA offers a simple and fast way to simulate discontinuities and reflections in traveling wave tubes.

To validate DIMOHA's simulations, we conducted an experimental study of reflections in TWT, where a defective TWT setup with varying standing wave ratio was achieved by attaching a mobile probe to a standard Ku-band TWT. Both simulations and measurements revealed a similar ripple effect in the saturated output power as a function of frequency.

Acknowledgements

We thank D. Minenna and A. Poyé for their crucial work on DIMOHA without which this study would not have been, as well as for our fruitful discussions. We also thank Philip Birtel for the valuable insights he provided. The Centre de

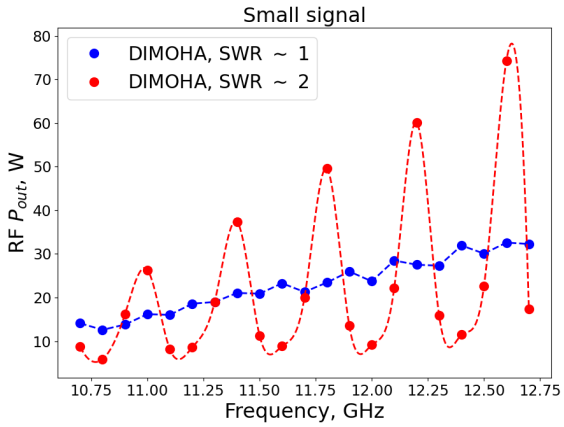

Fig. 10. Simulated RF output power as function of frequency in small signal regime for the standard and the maximum SWR setup (blue and red respectively).

Calcul Intensif d'Aix-Marseille is acknowledged for granting access to its high-performance computing resources.

REFERENCES

[1] T. M. Antonsen Jr, P. Safier, D. P. Chernin, and B. Levush, "Stability of traveling-wave amplifiers with reflections," *IEEE Transactions on Plasma Science*, vol. 30, no. 3, pp. 1089–1107, June 2002, 10.1109/TPS.2002.801563.

[2] P. Birtel, A. Jacob, W. Schwertfeger, J. David, and A. Le Clair, "Simulation of multi-reflections in a helix-type TWT," in *2008 IEEE International Vacuum Electronics Conference*. Monterey, CA, USA: IEEE, April 2008, pp. 298–299, 10.1109/IVELEC.2008.4556352.

[3] S. Wallander, "Reflexions and gain ripple in TWT's," *IEEE Transactions on Electron Devices*, vol. 19, no. 5, pp. 655–660, May 1972, 10.1109/T-ED.1972.17469.

[4] T. M. Antonsen Jr, D. P. Chernin, S. J. Cooke, and B. Levush, "Spurious reflection of space charge fields in TWTAs," *IEEE Transactions on Electron Devices*, vol. 52, no. 5, pp. 755–763, 2005.

[5] A. M. Cook, E. L. Wright, K. T. Nguyen, C. D. Joye, J. C. Rodgers, R. L. Jaynes, I. A. Chernyavskiy, F. N. Wood, B. S. Albright, D. K. Abe, J. P. Calame, B. Levush, D. E. Pershing, J. Atkinson, and T. Kimura, "Demonstration of a W-band traveling-wave tube power amplifier with 10-GHz bandwidth," *IEEE Transactions on Electron Devices*, vol. 68, no. 5, pp. 2492–2498, 2021.

[6] I. A. Chernyavskiy, T. M. Antonsen Jr, A. N. Vlasov, D. Chernin, K. T. Nguyen, and B. Levush, "Large-signal 2-d modeling of folded-waveguide traveling wave tubes," *IEEE Transactions on Electron Devices*, vol. 63, no. 6, pp. 2531–2537, 2016.

[7] P. Birtel, "Inclusion of multi-reflections in the beam-wave interaction simulation of traveling wave tubes," PhD Thesis, Technical University of Hamburg-Harburg, 2010.

[8] K. Aliane, Y. Elskens, F. André, and D. Minenna, "Many-particle models and short-pulse amplification in traveling wave tubes," *IEEE Transactions on Electron Devices*, vol. 68, no. 12, pp. 6476–6481, November 2021, 10.1109/TED.2021.3120969.

[9] D. Minenna, K. Aliane, Y. Elskens, A. Poyé, F. André, J. Puech, and F. Doveil, "Time simulation of the nonlinear wave–particle interaction in meters-long traveling-wave tubes," *Physics of Plasmas*, vol. 28, no. 9, p. 092110, September 2021, 10.1063/5.0059349.

[10] D. Mincnna, Y. Elskens, F. André, J. Puech, A. Poyé, F. Doveil, and T. Pereira, "DIMOHA: Traveling-wave tube simulations including band edge and multiple-carriers operations," in *2019 International Vacuum Electronics Conference (IVEC)*, April 2019, pp. 1–2.

[11] D. Minenna, Y. Elskens, F. André, A. Poyé, J. Puech, and F. Doveil, "DIMOHA: A time-domain algorithm for traveling-wave tube simulations," *IEEE Transactions on Electron Devices*, vol. 66, no. 9, pp. 4042–4047, September 2019, 10.1109/TED.2019.2928450.

[12] P. Bernardi, F. André, J. David, A. Le Clair, and F. Doveil, "Efficient time-domain simulations of a helix traveling-wave tube," *IEEE Transactions on Electron Devices*, vol. 58, no. 6, pp. 1761–1767, May 2011, 10.1109/TED.2011.2125793.